ADVANCED ENERGY MATERIALS
www.advenergymat.de

A Universal Additive Strategy to Reshape Electrolyte Solvation Structure toward Reversible Zn Storage

*Tian Chen Li, Yew Von Lim, Xue Liang Li, Songzhu Luo, Congjian Lin, Daliang Fang, Sunwen Xia, Ye Wang, and Hui Ying Yang**

The benefits of Zn, despite many of its performance advantages (e.g., high theoretical capacity and low redox potential), are compromised by severe side reactions and Zn dendrite growth in aqueous electrolytes, due to the coordinated H_2O within the Zn^{2+}-solvation sheath and reactive free water in the bulk electrolyte. Unlike most efforts focused on costly super-concentrated electrolytes and single additive species, a universal strategy is proposed to boost Zn reversibility in dilute electrolytes via adding carbonyl-containing organic solvents. Based on experimental investigations and multiscale simulations, the representative electrolyte with a *N*-methyl-2-pyrrolidone polar additive is proved to assist in structural reshaping of Zn^{2+}-solvation and stabilizing the hydrogen bond network of water. This synergy is instrumental in contributing to suppressed water-induced parasitic reactions and dendrite formation, which enables high average coulombic efficiency of 99.7% over 1000 cycles in an Zn/Cu asymmetric cell, and an ultralong cycling lifespan of 2000 cycles with 99.4% capacity retention in a Zn/VS_2@SS full cell. Even with an elevated cathodic mass loading (up to 9.5 mg cm^{-2}), the cycling stability is still maintained. The proposed strategy provides new insight into electrolyte additive design and sheds light on high-performance Zn-ion batteries.

1. Introduction

The increasing demand in green energies and alternatives requires urgent development of reliable and safe energy storage systems.[1] As one of the potential candidates, aqueous zinc-ion batteries (AZIBs) received widespread attention due to their low cost, high theoretical capacity (820 mAh g^{-1}), intrinsic safety and environmental benignity.[2,3] Despite these attractive merits, the performance is largely limited by unstable Zn chemistry in aqueous electrolyte with mildly acidic environment.[4–6] The produced hydrated $[Zn(H_2O)_x]^{2+}$ ion complex species and the free water outside the Zn^{2+}-solvation sheath induce severe interfacial side reactions, including Zn corrosion and H_2 evolution, along with aggravation of nonuniform Zn deposition.[7–9] This inevitably results in low Coulombic efficiency (CE) and can ultimately compromise safety (e.g., battery swelling and explosion, short-circuit failure).[10]

To circumvent the problems, many attempts have been made, including Zn alloying,[11] surface modification,[12,13] structure optimization of Zn host,[14,15] adoption of Zn^{2+} intercalation anode material,[16,17] and compositional design of electrolyte.[18–20] Among them, electrolyte design is the most expedient solution with the potential to scale up from lab to practical application, owing to its superior repeatability and diversity. Recently, super-concentrated electrolytes are explored to interrupt original solvated balance and improve Zn reversibility.[21–24] The most representative example was proposed by Wang et al., where the Zn^{2+} is surrounded by bis(trifluoromethanesulfonyl) imide ($TFSI^-$) instead of water molecules due to the formation of copious $[Zn(TFSI)]^+$ ionic pairs with close coordination.[25–28] However, a high concentration of reaction-unrelated salt or flammable organic species in the electrolyte may induce safety and reaction kinetic issues with occurring costs, going against the initial rationale behind using AZIBs.[29] As such, investigations now are focusing on developing electrolyte additives on Zn^{2+}-solvation structure in dilute solutions, such as methanol,[30] polyhydric alcohols,[31,32] dimethyl sulfoxide,[33,34] and polyacrylamide.[35] Although the Zn deposition behavior is optimized, many organic additives are still plagued by limited alleviation of side reactions.[10] Meanwhile, most of them hugely increase the polarization voltage while improving the cycling stability, leading to inferior electrochemical performance under practical conditions with high current density and areal capacity. Currently, rationally developing a class of advanced multifunctional additives remains challenging and a general additive design principle is accordingly of great significance for aqueous Zn chemistry.

Carbonyl-containing liquid organics, such as *N*-methyl-2-pyrrolidone (NMP), *N*,*N*-dimethylformamide (DMF), and acetone

T. C. Li, Y. V. Lim, X. L. Li, C. Lin, D. Fang, S. Xia, H. Y. Yang
Pillar of Engineering Product Development
Singapore University of Technology and Design
8 Somapah Road, Singapore 487372, Singapore
E-mail: yanghuiying@sutd.edu.sg
S. Luo
School of Materials Science and Engineering
Nanyang Technological University
50 Nanyang Avenue, Singapore 639798, Singapore
Y. Wang
Key Laboratory of Material Physics
Ministry of Education
School of Physics and Microelectronics
Zhengzhou University
Zhengzhou 450052, China
The ORCID identification number(s) for the author(s) of this article can be found under https://doi.org/10.1002/aenm.202103231.

DOI: 10.1002/aenm.202103231

(DMK), are strongly polar solvents. These water-miscible additives can serve as the proton acceptor bonding with dipolar water molecules and destroy the original water clusters in the aqueous solution. In addition, they are prone to preferentially solvate Zn^{2+} cations due to the high polarity.[36] Inspired by this, herein, we propose a universal strategy to achieve Zn reversibility by introducing carbonyl-containing organic polar solvents into the $ZnSO_4$-based electrolyte. With comprehensive analysis including experimental and theoretical studies, these organic molecules are proven to participate in the solvated Zn^{2+} sheaths and replace coordinated H_2O, which renders less H_2O involved in the anodic interfacial reaction during cycling. Meanwhile, the strong interaction between H_2O and NMP reduces the population of free water outside the solvation sheath and contributes to the mitigation of spontaneous side reactions in aqueous $ZnSO_4$ electrolyte. As a result, reversible Zn plating/stripping with a high CE of 99.7% is achieved in the prepared electrolyte. Moreover, the assembled Zn/VS_2@SS full battery shows exceptional cycling stability (2000 cycles, 99.4% capacity retention at 1 A g^{-1}), with inhibited Zn interfacial issues even at high cathodic mass loading (9.5 mg cm^{-2}).

2. Results and Discussions

In general, high-polarity solvents give rise to dissociation of salts and strong affinity with charged metal ions, thus enhancing battery performance.[37,38] NMP, as a highly polar aprotic solvent with one hydrogen bond (H-bond) acceptor (carbonyl functional group), can limit the intermolecular interaction between H_2O and realize reconstruction of three-dimensional H-bond network.[36] In contrast to carbonyl-containing DMF and DMK molecules, NMP features with the largest solvent dipole moment (4.09) and relatively high dielectric constant (33.0), facilitating insertion into the Zn^{2+}-solvation sheath and replacement of coordinated H_2O (**Figure 1**a).[39] Moreover, the calculated electrostatic potential (ESP) mapping of NMP demonstrates the highest electronegativity (−5.135 eV), validating the strongest interaction to H_2O/cation among them (Figure S1, Supporting Information). Therefore, NMP was chosen as an example to verify the feasibility of this tactic in the following section.

To study the impact of NMP additive on the $ZnSO_4$ electrolyte, a series of electrolytes with NMP volume ratio (VR) ranging from 0% to 50% was prepared, denoted as NMP0, NMP2, NMP5, NMP10, and NMP50, respectively. No apparent delamination is observed when VR reaches 10%, indicating a robust structure. As VR reaches 50% (NMP50), zinc salt precipitation and recrystallization are shown (Figure S2, Supporting Information). The ionic conductivity was measured by conductivity meter. Among these electrolytes, the additive-free 2 M $ZnSO_4$ electrolyte exhibits the best ionic conductivity (49.0 mS cm^{-1}), and a slight decline of ionic conductivity is noted with the increase of NMP VR.[7] This might be attributed

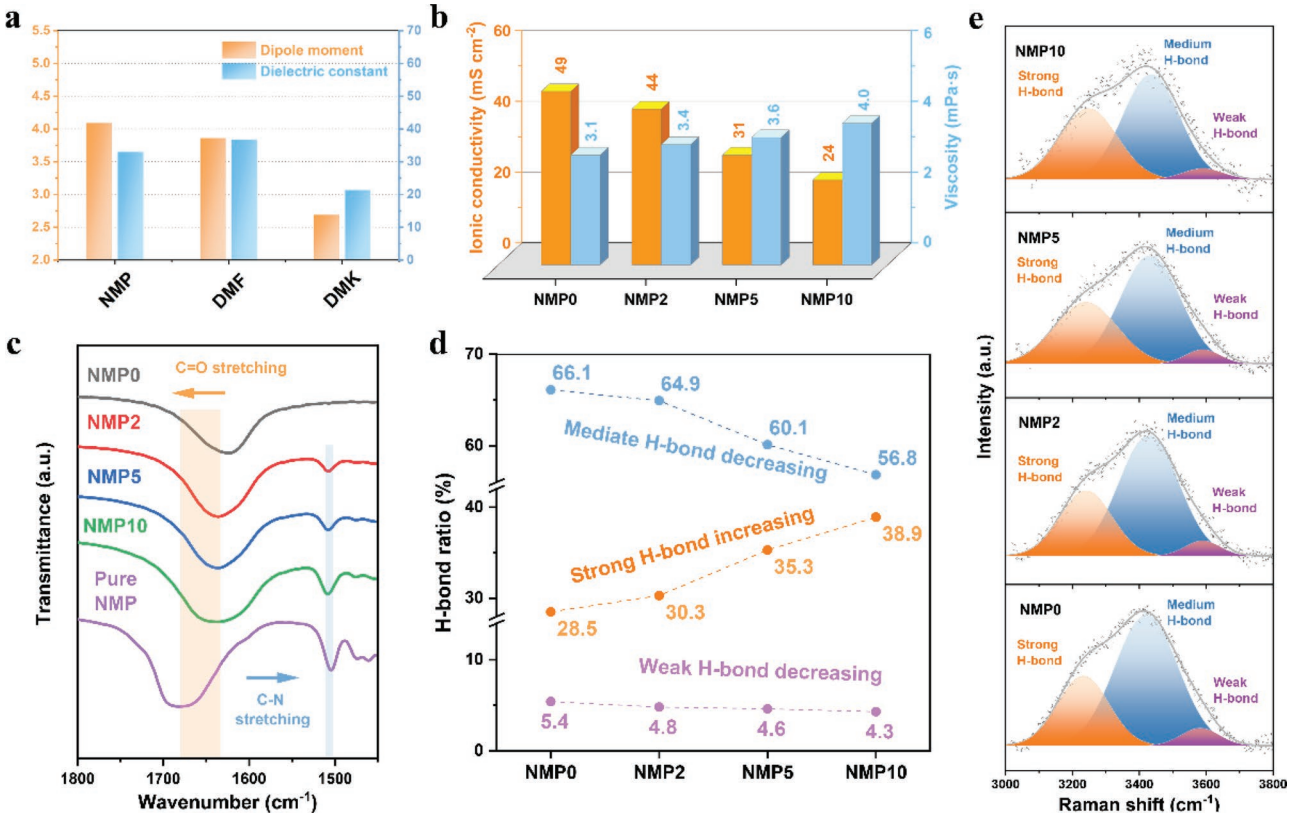

Figure 1. Physical properties and spectral studies of carbonyl-containing organic additives. a) Dipole moment and dielectric constant of NMP, DMF, and DMK. b) Measured ionic conductivity and viscosity of the electrolytes. c) FTIR spectra of the electrolytes with NMP additive. d) The proportions of strong, mediate, and weak H-bond in the electrolytes. e) Fitted Raman spectra of the electrolytes in the region of O—H stretching.

to changed coordination environment in the presence of additives. Conversely, the viscosity gradually increases as NMP content increases (Figure 1b).

To practically probe the Zn^{2+}-solvation structure, Fourier transform infrared spectroscopy (FTIR) and Raman spectroscopy were performed. FTIR results indicate the C=O stretching vibration (1600–1700 cm^{-1}) shifts to higher wavenumbers with increasing NMP content (Figure 1c). This is due to the coordination interaction between NMP and water molecules, which can be evidenced by H-bond induced blueshift of the C—N stretching vibration and redshift of C—H stretching vibration in the presence of NMP (Figure S3, Supporting Information). The reconstructed H-bond network is also supported by the Raman spectroscopic investigation, where the C=O stretching vibration shows redshift with the increase of NMP content (Figure S4, Supporting Information), and gradually approaches the peak location of pure NMP (1675 cm^{-1}). For the O—H stretching vibration within the region from 3000 to 3800 cm^{-1}, it can be divided into three characteristic peaks, corresponding to strong, mediate, and weak H-bond, respectively (Figure 1e).[40,41] Based on the deconvoluted peak area, the H-bond proportions of various electrolytes are summarized (Figure 1d). The proportion of mediate and weak H-bonds located at higher frequency shows downward trend, whereas that of strong H-bond with lower bond energy gradually increases with increasing NMP content. These results indicate that NMP additive can stabilize the water cluster via stronger H-bond interaction and decrease the population of free water in the bulk electrolyte. In addition, we also rationally designed series of $ZnSO_4$-based aqueous electrolytes with various content of other organic carbonyl compound additives, including DMF and DMK. Similarly, mixing $ZnSO_4$ solution with these two solvents results in blueshift of C=O stretching vibration in contrast to the corresponding pure solvents, demonstrating the effectiveness of carbonyl-containing additives in disturbing the original coordination balance and structural reshaping of Zn^{2+}-solvation (Figure S5, Supporting Information).

Molecular dynamics (MD) simulations were performed to further elucidate the Zn^{2+}- solvation structure of the systems with/without NMP additive. As shown, five molecules of H_2O and one SO_4^{2-} anion are coordinated with one Zn^{2+} in the case of blank electrolyte (**Figure 2**a). In comparison, two coordinated H_2O molecule is substituted by NMP molecules for the NMP5 cell (Figure 2b). To analyze the solvation structure in depth, corresponding radial distribution functions (RDFs) and coordination number (CN) distribution functions were attempted. NMP0 electrolyte shows a sharp Zn-O_{H2O} peak at ≈2.1 Å, suggesting a structured arrangement of H_2O around Zn^{2+} ions in the solvation shell. In the NMP5 cell, however, a new peak corresponded to Zn-O_{NMP} pair appears at the same position of Zn-O_{H2O} peak, indicating insertion of NMP molecules into the solvation shell (Figure S6, Supporting Information). Supplementary structural information can be obtained from the analysis of CN. The Zn^{2+}-solvation shell in NMP5 electrolyte is occupied by 2.7 H_2O and 2.0 NMP molecules on average (Figure 2d), and the dominant ionic solvation cluster is thereby confirmed in the form of $[Zn(H_2O)_3(NMP)_2]^{2+}$, which is in agreement with the simulated structure displayed above. This implies the differences from conventional $ZnSO_4$ electrolyte, where one Zn^{2+} cation is associated with 5.4 dipolar H_2O, that is $[Zn(H_2O)_5]^{2+}$ solvation structure (Figure 2c).

Density functional theory (DFT) calculation was performed to understand the interaction from the atomic-level scale. The binding energy of Zn^{2+}-H_2O pair and Zn^{2+}-NMP pair were calculated to be −4.512 and −5.492 eV, respectively (Figure 2e). The stronger interaction between cationic Zn^{2+} and electronegative carbonyl oxygen from NMP reveals the preferential involvement of NMP in the Zn^{2+}-solvation structure. Moreover, NMP-H_2O pair exhibits high binding energy of −3.726 eV, which is lower than H_2O-H_2O pair of −2.943 eV (Figure 2e). This implies the original water H-bond network tends to reorganize, and more free water is captured and bonded with polar NMP molecules. Consequently, the population of free water is reduced, which is consistent with the spectral analysis. As another reliable analysis method, ESP mapping was utilized to visualize the charge distribution around the Zn^{2+}-solvation structures. In the additive-free $ZnSO_4$ electrolyte, ESP of the hydrated $[Zn(H_2O)_5]^{2+}$ is high (Figure 2f). In comparison, that of the $[Zn(H_2O)_3(NMP)_2]^{2+}$ is decreased after the introduction of NMP additive, which indicates alleviated repulsion force surrounding the reorganized Zn^{2+}-solvation structure and may contribute to accelerated ionic migration (Figure 2g).[42] However, on the other hand, the insertion of NMP inevitably enlarge the size of solvated ion complex, leading to sluggish ion-transfer kinetics and higher interfacial desolvation energy barrier. As a result, the charge transfer resistance is slightly increased in NMP5 electrolyte (Figure S7, Supporting Information).

To find the optimal electrochemical performance, the Zn plating/stripping stability was analyzed via Zn/Zn symmetric cells. The symmetric cell with NMP0 electrolyte fails at 80 h with a sudden polarization voltage fluctuation at a current density of 1 mA cm^{-2} with the capacity of 1 mAh cm^{-2}. In contrast, with an amount of 5 vol% NMP addition, the symmetric cell cycles over 540 h, which is near seven times as long as NMP0 electrolyte (**Figure 3**a). Moreover, the symmetric cells with NMP2 and NMP10 electrolytes exhibit cycle life of 450 and 370 h, respectively (Figure S8, Supporting Information). This indicates NMP5 electrolyte features optimal solvation structure and cycling performance among the electrolytes with NMP additive. The cycling stability of Zn was further evaluated at a strict condition (5 mA cm^{-2}, 5 mAh cm^{-2}). The introduced NMP additive has few impacts on the polarization voltage and displays a stable voltage profile for 195 h, whereas the additive-free electrolyte can only achieve cycle life of ≈50 h (Figure S9, Supporting Information). As acknowledged in the previous literatures, inhomogeneous ion concentration and electric field distribution during battery operation generally trigger nonuniform nucleation and dendrite growth,[10] which is evidenced by the scanning electron microscopy (SEM) image of Zn anode after 50 cycles in pure $ZnSO_4$ electrolyte (Figure 3e). Benefited from the NMP additive, protruded Zn deposits are absent in the case of NMP5 electrolyte, suggesting modulated deposition behavior without unfavorable dendrite formation (Figure 3f). Even after 100 cycles, the Zn electrode in NMP5 electrolyte still shows no Zn protuberance (Figure S10, Supporting Information), and maintains a smooth surface topology with low surface roughness of 0.15 μm (Figure S11, Supporting Information).

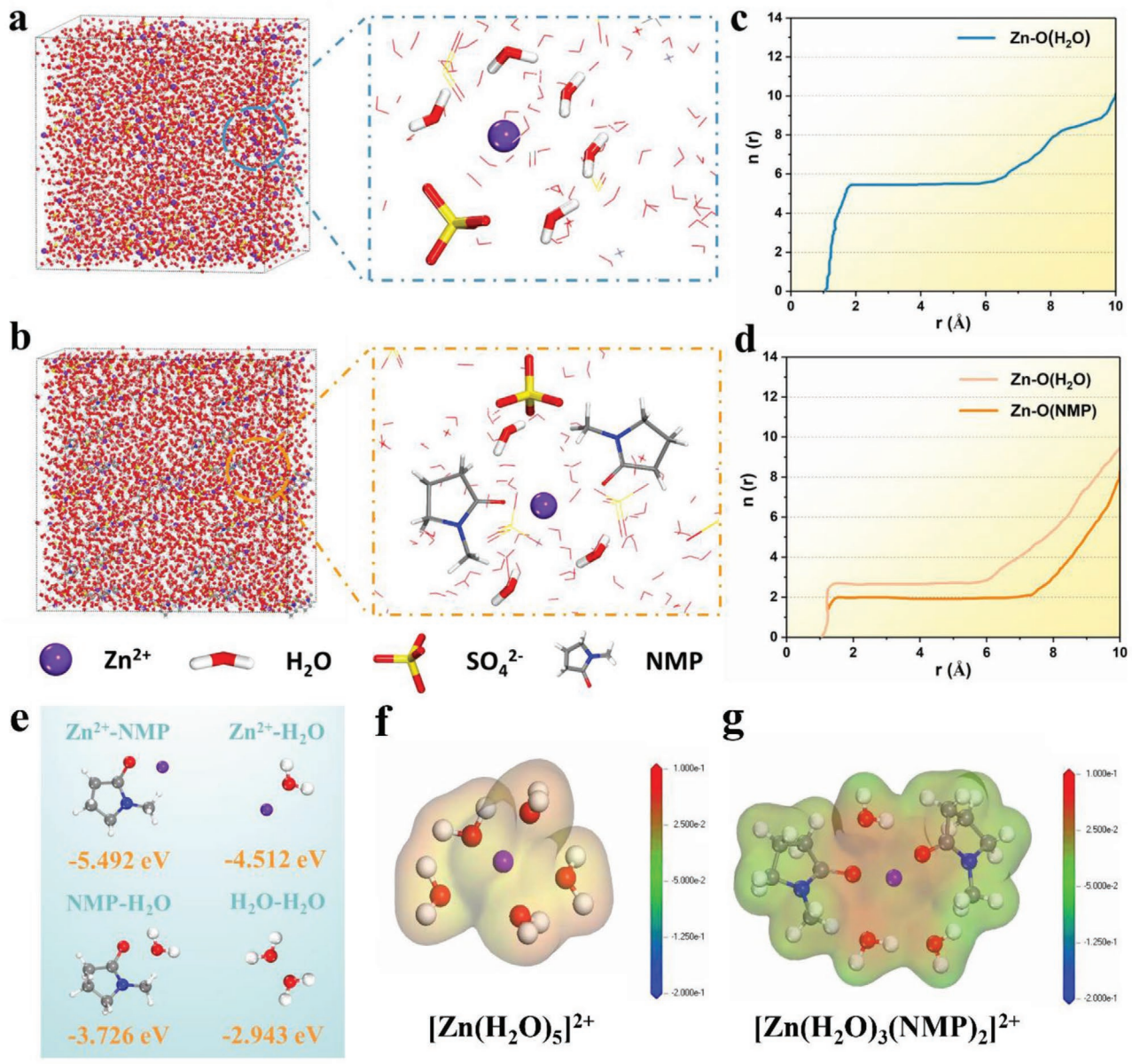

Figure 2. Theoretical investigations of the additive-free $ZnSO_4$ electrolyte and NMP-introduced electrolytes. Snapshots of the MD simulation cells and representative solvation structures in the electrolytes with a) NMP0 and b) NMP5 electrolytes. Coordination number of Zn—O bond for c) NMP0 and d) NMP5 electrolytes. e) DFT-calculated binding energies of various pairs. ESP distribution of f) pristine and g) modulated Zn^{2+}-solvation structures. Red and blue colors of the scale bar reflect higher and lower potential, respectively.

Since CE is an important performance metric for realizing commercialization, CEs of the Zn/Cu asymmetric cells using NMP0 and NMP5 electrolytes were evaluated. The cell using pristine $ZnSO_4$ first experiences a lattice fitting process with 79.8% initial CE,[42] and finally fails after 134 h at a current density of 1 mA cm^{-2}. For the cell with NMP5 electrolyte, however, it achieves a higher initial CE (81.7%) and maintains a superior average CE of 99.7% over up to 1000 cycles (Figure 3b–d). In contrast, the cycle life of NMP2 and NMP10 is 380 and 180 h, respectively, with a lower average CE than the case of NMP5 (Figure S12, Supporting Information). Digital pictures were taken to observe the morphology evolution of Cu and Zn electrodes stripped from Zn/Cu asymmetric cells after 50th plating (Figure S13, Supporting Information). The images show that the Cu electrode cycled in NMP0 electrolyte suffers from nonuniform Zn deposition. As a result, some glass fibers are pierced through by rigid Zn tips and tightly attached to the Cu surface. Moreover, the Zn electrode is plagued by the parasitic reactions, with severely corroded surface. In contrast, uniform Zn is shown to deposit on Cu electrode in the case of NMP5 electrolyte with indiscernible dendrite formation, and uncontrolled Zn corrosion in acidic aqueous solution is effectively mitigated. The SEM images of Cu electrodes after 50th plating are shown in Figure 3g,h. Consistent to the observation, the

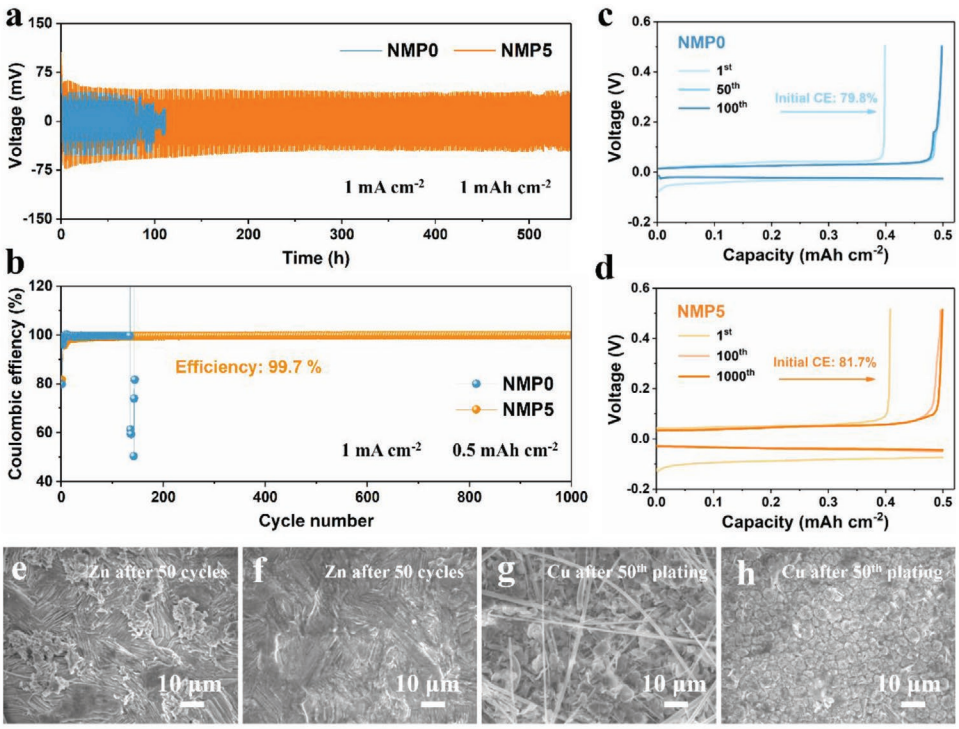

Figure 3. Comparison of electrochemical Zn/Zn^{2+} redox reaction in NMP0 and NMP5 electrolytes. Cycling stability of a) Zn/Zn symmetric cells and b) Zn/Cu asymmetric cells. Voltage profiles of Zn/Cu asymmetric cells using c) NMP0 and d) NMP5 electrolytes at various cycles. SEM images of Zn electrodes stripped from Zn/Zn cells using e) NMP0 and f) NMP5 electrolytes after 50 cycles. SEM images of Cu electrodes stripped from Zn/Cu cells using g) NMP0 and h) NMP5 electrolytes after 50th plating.

Cu electrode cycled in NMP5 electrolyte displays uniform Zn deposits than the NMP0 case, which facilitates highly reversible Zn electrochemistry. CEs of Zn/Cu cells were subsequently investigated at a higher current density of 2 mA cm^{-2} and an areal capacity of 1 mAh cm^{-2} (Figure S14, Supporting Information). Inferior cyclability and CE are revealed in the electrolyte without NMP. In the NMP5 electrolyte, however, the asymmetric cell cycles over 600 h with a high average CE of 99.8%. The superior electrochemical performances, including CE and cycling stability, outperform most reported electrolyte additives under similar test conditions (Table S1, Supporting Information), demonstrating the practical potential of NMP additive in reversible Zn batteries.

Apart from the NMP additive, Zn reversibility of $ZnSO_4$-based aqueous electrolytes with various content of DMF and DMK were evaluated. Symmetric cells with DMF5 and DMK5 electrolytes show the best cycling stability in their respective systems, with battery life of 420 and 500 h, respectively (Figures S15 and S16, Supporting Information). When assembled in Zn/Cu cells, DMF5 and DMK5 realize stable CEs and long-term plating/stripping (Figure S17, Supporting Information). The improved reversibility is ascribed to negatively charged carbonyl group in these two organic compounds, rendering electrolyte solvation structures reshaped. These results indicate the versatility of the carbonyl-containing additive strategy to stabilize the Zn/electrolyte interface in achieving prolonged cycling lifespan of Zn anode.

A homemade in situ optical system was constructed to visually observe the Zn electroplating process (Figure S18, Supporting Information). In NMP0 electrolyte, abundant gas bubbles accumulate on Zn surface after 8 min plating, arising from the severe side reactions. Moreover, Zn protrusions are visible with the gradual increase of plating capacity and ultimately grow into ramified Zn dendrites (**Figure 4**a). In contrast, dense and even Zn surface can be achieved in NMP5 electrolyte without discernible H_2 evolution (Figure 4b). Modulated Zn deposition can be verified by chronoamperometry (CA) results, where Zn in NMP0 electrolyte exhibits a typical 2D diffusion pattern with decreasing exchange current density, corresponding to inhomogeneous Zn nucleation and vertical growth of dendrites. In comparison, a constant 3D diffusion process is revealed in NMP5 electrolyte after a short nucleation stage for 30 s, demonstrating smooth surface morphology is maintained over the 180 s plating (Figure 4c).[43] Nucleation overpotential analysis of Zn/Ti asymmetric cells provide additional insight into the Zn deposition behavior. As presented in Figure 4d, the initial nucleation overpotential of Zn in NMP5 electrolyte is 55.2 mV, which is increased by 17.7 mV than that of NMP0 electrolyte. This higher energy barrier means a stronger driving force (overpotential) is required for the initial nucleation stage, and consequently, facilitating more uniform Zn deposition with fine grain size (Figure 2h).[44,45] The smooth plating behavior also benefited from improved hydrophilicity of NMP5 electrolyte, since rapid and complete electrolyte wetting on Zn surface is advantageous for the homogeneity of zinc-ion flux (Figure S19, Supporting Information).[8]

Undesired reactions, including interfacial corrosion and H_2 evolution, are thermodynamically favorable in the baseline

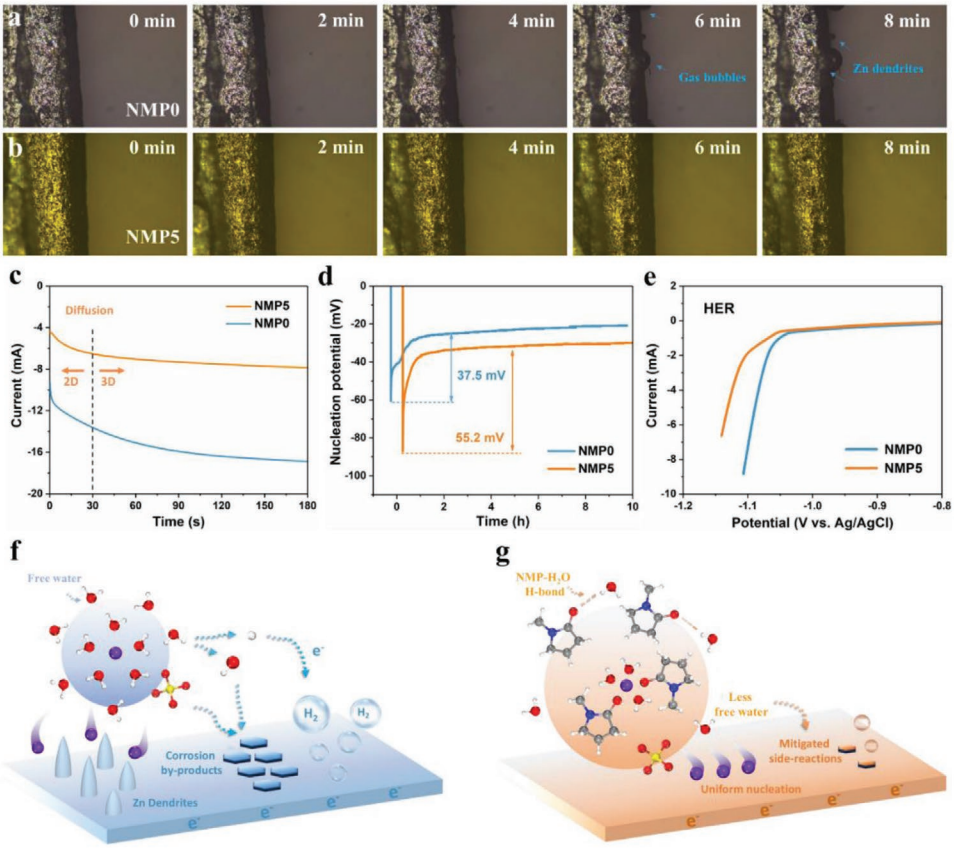

Figure 4. Mechanistic insight of NMP electrolyte additive. In situ optical visualization observations of the Zn deposition process in a) NMP0 and b) NMP5 electrolytes. c) CA of Zn/Zn symmetric cells, d) initial Zn nucleation overpotential of Zn/Ti cells at 1 mA cm^{-2}, and e) LSV characterization in the electrolytes. Schematic illustration of the Zn^{2+}-solvation structure and corresponding deposition behavior in f) NMP0 and g) NMP5 electrolytes.

electrolyte according to the Pourbiax diagram ($3Zn + ZnSO_4 + 11H_2O \rightarrow Zn_4SO_4(OH)_6 \cdot 5H_2O + 3H_2$).[8] Water decomposition during charging ($2H^+ + 2e^- \rightarrow H_2$) further exacerbates the precipitation of insulating by-products and reduce Zn reversibility. To evaluate the inhibition effect of NMP on parasitic reactions, linear sweep voltammetry (LSV) test was performed. As shown in Figure 4e, the response current density of NMP5 electrolyte is much lower than that of pure $ZnSO_4$ electrolyte, implying the improved electrochemical stability of water resulted from optimized electrolyte solvation structure. Evaluated Tafel curves demonstrate corrosion suppression capability of NMP5 electrolyte during cycling (Figure S20, Supporting Information). Compared with NMP0 electrolyte, Zn in NMP5 electrolyte exhibits more positive corrosion potential (–1.007 V vs the saturated calomel electrode) and lower current density (-4.89×10^{-3} mA cm^{-2}). Such excellent anticorrosion performance can be confirmed by the X-ray diffraction (XRD) patterns of Zn after cycling (Figure S21, Supporting Information). For the NMP5 electrolyte, irreversible corrosion by-products are undetectable after 100 cycles. As comparison, the diffraction peak intensity gradually increases from 0 to 100 cycles without additive. Complementary support comes from the soaking experiment results, where copious hexagonal-shaped by-products were attached to Zn surface after soaking in pure $ZnSO_4$ electrolyte for 5 d, while no obvious corroded surface feature was observed in the designed NMP5 electrolyte (Figure S22, Supporting Information). This result is in agreement with the energy dispersive spectroscopy (EDS) mapping (Figure S24, Supporting Information). Based on the XRD patterns, phase constitution of these by-products was identified as $Zn_4SO_4(OH)_6 \cdot xH_2O$ (Figure S23, Supporting Information). Moreover, the weaker peak intensity of by-products for NMP5 electrolyte further validates alleviation of spontaneous corrosion issue and parasitic H_2 evolution.

Combining the experimental and theoretical results, the working mechanism of NMP additive can be comprehensively understood. It has been acknowledged that Zn^{2+} ions exist in the aqueous electrolyte as hydrated $[Zn(H_2O)_5]^{2+}$ or $[Zn(H_2O)_6]^{2+}$ species. The central Zn^{2+} ions serve as Lewis acid sites can hydrolyze H_2O to generate H^+ protons and induce side reactions in such a mildly acidic environment.[34,46] As a long-lasting problem for metal electrodes, dendrite growth is another unfavorable phenomenon during battery operation caused by the "tip effect" (Figure 4f).[47] After introducing NMP additive, the electrolyte coordination environment is changed, and the Zn deposition behavior is thereby modulated. To be specific, the H_2O molecules in the solvation shell are partly replaced by the highly polar NMP molecules. Simultaneously, original H-bond interaction between H_2O is disrupted and more free water molecules in the outer sheath are trapped by carbonyl-containing NMP. Thus, the water-induced parasitic reactions are mitigated, due to less H_2O molecules involved in

the interfacial reactions and the lower proton activities. Additionally, by virtue of the unique structural arrangement of solvated $[Zn(H_2O)_3(NMP)_2]^{2+}$ complex, slightly higher overpotential is required for Zn nucleation. Consequently, uniform nuclei distribution and dendrite-free Zn deposition are realized (Figure 4g). The regulation mechanism proposed here is also applicable to DMF and DMK because of their proton acceptor ability with the help of their electronegative carbonyl oxygen. To summarize, the carbonyl-containing polar solvents serve as a class of attractive multifunctional additives that can to a great extent circumvent uncontrolled Zn growth and adverse reactions via structural reshaping of the electrolyte solvation, thereby ensuring stable long-term cycling.

To exemplify the practical application potential of the designed electrolyte, full cells based on VS_2 electrode and Zn foil were assembled. The VS_2 nanosheets were directly grown on stainless steel mesh (SS) as free-standing cathode via hydrothermal reaction (Figure S25, Supporting Information).[48] The cyclic voltammetry curves of the Zn/VS_2@SS battery are displayed in Figure S26 in the Supporting Information. Two couples of cathodic/anodic peaks can be identified for full batteries in the two different electrolytes, corresponding to the two-stage Zn^{2+} insertion/extraction process.[49] This is supported by the XPS spectra of VS_2, where the Zn 2p signals occur when discharged to 0.4 V, while the intensity dramatically decreases after subsequent charging (Figure S27, Supporting Information). Moreover, EDS elemental mappings of the discharged samples clearly reveal uniform distribution of Zn, further confirming Zn^{2+} insertion into the interlamination of VS_2 (Figure S28, Supporting Information).

The cycling stability of Zn/VS_2@SS batteries was characterized at a current density of 1.0 A g^{-1} with a cathode mass loading of ≈5.3 mg cm^{-2} (**Figure 5**a). The NMP0 cell delivers

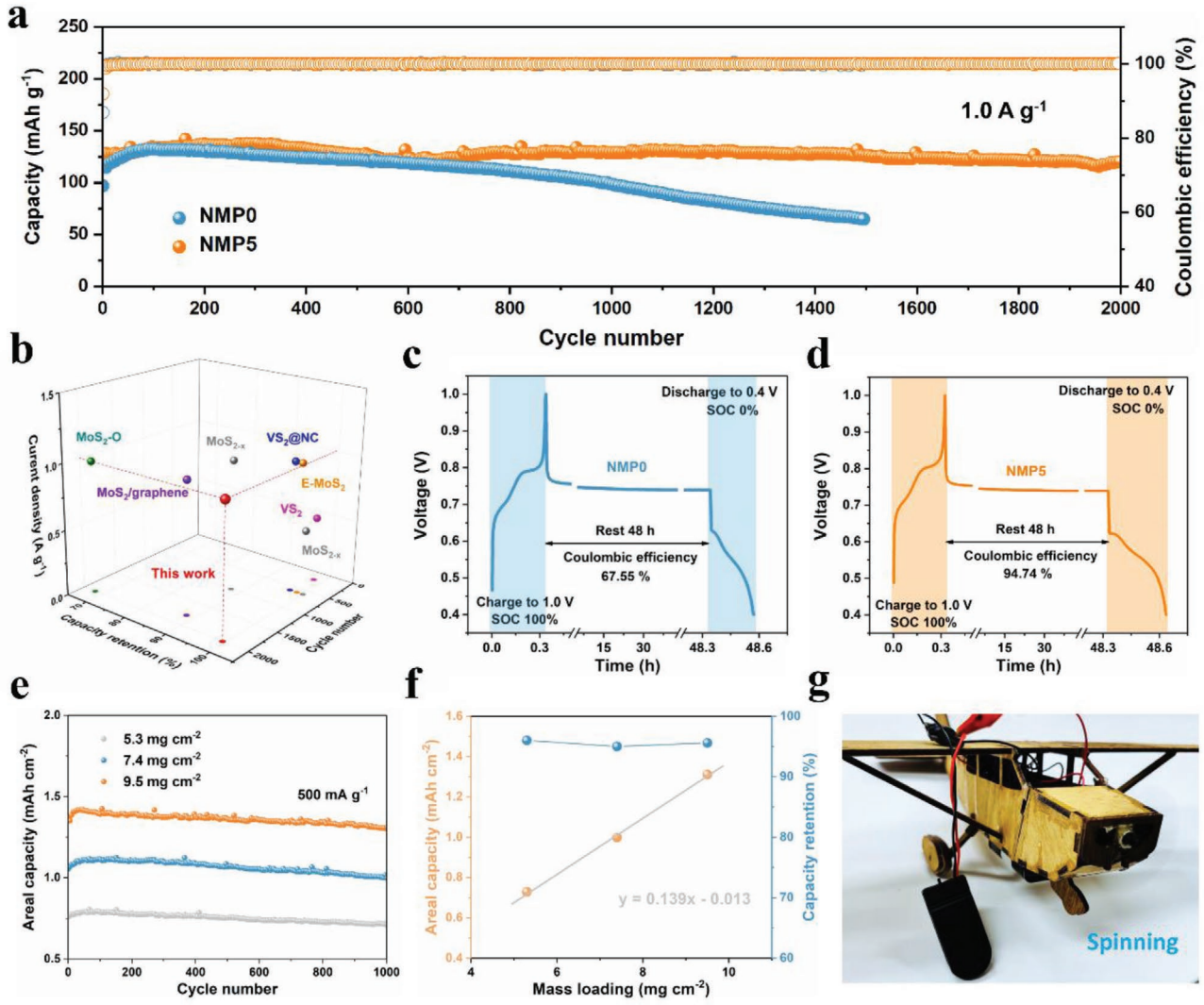

Figure 5. Electrochemical performance of Zn/VS_2@SS full cells using NMP0 and NMP5 electrolytes. a) Long-term cycling of the assembled batteries at a current density of 1.0 A g^{-1}. b) Comparison of the current density, capacity retention, and cycle number between Zn/VS_2@SS full cells and other reported sulfide-based Zn batteries. Self-discharge analysis of cells using c) NMP0 and d) NMP5 electrolytes. e) Cycling stability of Zn/VS_2@SS full cells with increasing mass loading from 5.3 to 9.5 mg cm^{-2}. f) Relationship between two metrics (areal capacity, capacity retention) and cathodic mass loading. g) The spinning propeller of a homemade aircraft model powered by two coin cells.

an initial capacity of 97 mAh g^{-1} with the 1st CE of 86.9% and decays rapidly after 800 cycles. In contrast, owing to the mitigated side reactions of Zn, as well as the controlled dendritic growth (Figure S29, Supporting Information), the cell with NMP5 exhibits a higher initial CE of 91.8% and an ultralong operational lifetime with 99.4% capacity retention after 2000 cycles. It also shows superior cycling lifespans over 1500 cycles with 0.009% capacity fading per cycle at 500 mA g^{-1}, versus NMP0 cell (≈600 cycles), accompanied by the strong fluctuation of CEs (Figure S30, Supporting Information). The cycling performance is superior to almost all reported Zn batteries based on metal sulfides in terms of cycle number and capacity retention (Figure 5b, details in Table S2, Supporting Information), such as VS_2 (98%, 200 cycles at 500 mA g^{-1}),[49] VS_2@NC (97%, 600 cycles at 1 A g^{-1}),[50] and MoS_{2-x} (87.8%, 1000 cycles at 1 A g^{-1}).[51] The battery self-discharge can be reflected by the CEs of fully charged batteries after 2 d rest. A CE of 94.74% is achieved in the cell with NMP5 electrolyte (Figure 5c), while only 67.55% capacity is retained for the cell without NMP additive (Figure 5d). To meet the commercial-grade requirement, VS_2@SS cathodes with elevating mass loading from 5.3 to 9.5 mg cm^{-2} were synthesized (Figure S31, Supporting Information). All cells using NMP5 electrolyte achieve outstanding long-term cycling with high CEs of ≈100% and slow capacity decay over 1000 cycles without being influenced by the increased cathodic loading mass, indicating unstable anode/electrolyte interface under harsh test conditions is effectively controlled (Figure 5e). This is directly reflected in the linearly correlated capacity with rather small standard error. (Figure 5f). With this high areal capacity, the supplied energy from two coin cells enables to power a small propeller device. (Figure 5g).

3. Conclusion

By mixing carbonyl-containing organic solvents with $ZnSO_4$ aqueous solution, we develop a general low-cost tactic to regulate the aqua cationic Zn species and the coordination environment of water molecules. Specifically, spectral studies and theoretical simulations reveal that the representative NMP molecules in NMP5 electrolyte can insert into the inner Zn^{2+}-solvation shell, inducing the transformation of original $[Zn(H_2O)_5]^{2+}$ to less hydrated $[Zn(H_2O)_3(NMP)_2]^{2+}$ species. This enables uniform Zn deposition and alleviated interfacial side reactions. Concomitantly, the free water outside the solvation sheath is partly confined by NMP additive through H-bond, leading to reduced water activity. With this solvation modulation, Zn anode shows a sevenfold increase in cycle life in Zn/Zn symmetric cells at a current density of 1 mA cm^{-2} and high Zn utilization (99.7%) over 1000 cycles in Zn/Cu asymmetric cells. With the excellent reversibility, the Zn/VS_2@SS full batteries exhibit ultrastable cycling performance over 2000 cycles with 99.4% capacity retention and can withstand the exacerbated interface instability brought by high cathodic mass loading. Such superior electrochemical performance outperforms almost all reported Zn/metal sulfide batteries and provides a new possibility for high-performance commercial AZIBs.

Supporting Information

Supporting Information is available from the Wiley Online Library or from the author.

Acknowledgements

The research project was supported by the Ministry of Education, Singapore, under its MOE tier2 grant MOE2019-T2-1-181.

Conflict of Interest

The authors declare no conflict of interest.

Data Availability Statement

The data that support the findings of this study are available from the corresponding author upon reasonable request.

Keywords

electrolyte additives, *N*-methyl-2-pyrrolidone, organic carbonyl compounds, solvation structure regulation, zinc-ion batteries

Received: October 18, 2021
Revised: January 24, 2022
Published online:

[1] D. L. Chao, W. H. Zhou, F. X. Xie, C. Ye, H. Li, M. Jaroniec, S. Z. Qiao, *Sci. Adv.* **2020**, *6*, eaba4098.
[2] X. Xie, S. Liang, J. Gao, S. Guo, J. Guo, C. Wang, G. Xu, X. Wu, G. Chen, J. Zhou, *Energy Environ. Sci.* **2020**, *13*, 503.
[3] J. T. Huang, J. Zhou, S. Q. Liang, *Acta Phys. Chim. Sin.* **2021**, *37*, 2005020.
[4] M. E. Pam, D. Yan, J. Z. Yu, D. L. Fang, L. Guo, X. L. Li, T. C. Li, X. Y. Lu, L. K. Ang, R. Amal, Z. J. Han, H. Y. Yang, *Adv. Sci.* **2021**, *8*, 2002722.
[5] V. Verma, S. Kumar, W. Manalastas, M. Srinivasan, *ACS Energy Lett.* **2021**, *6*, 1773.
[6] J. W. Gao, X. S. Xie, S. Q. Liang, B. A. Lu, J. Zhou, *Nano-Micro Lett.* **2021**, *13*, 69.
[7] L. Ma, Q. Li, Y. Ying, F. Ma, S. Chen, Y. Li, H. Huang, C. Zhi, *Adv. Mater.* **2021**, *33*, 2007406.
[8] C. X. Liu, X. S. Xie, B. G. Lu, J. Zhou, S. Q. Liang, *ACS Energy Lett.* **2021**, *6*, 1015.
[9] X. H. Zeng, K. X. Xie, S. L. Liu, S. L. Zhang, J. N. Hao, J. T. Liu, W. K. Pang, J. W. Liu, P. H. Rao, Q. H. Wang, J. F. Mao, Z. P. Guo, *Energy Environ. Sci.* **2021**, *14*, 5947.
[10] T. C. Li, D. L. Fang, J. T. Zhang, M. E. Pam, Z. Y. Leong, J. Z. Yu, X. L. Li, D. Yan, H. Y. Yang, *J. Mater. Chem. A* **2021**, *9*, 6013.
[11] S.-B. Wang, Q. Ran, R.-Q. Yao, H. Shi, Z. Wen, M. Zhao, X.-Y. Lang, Q. Jiang, *Nat. Commun.* **2020**, *11*, 1634.
[12] J. N. Hao, B. Li, X. L. Li, X. H. Zeng, S. L. Zhang, F. H. Yang, S. L. Liu, D. Li, C. Wu, Z. P. Guo, *Adv. Mater.* **2020**, *32*, 202003021.
[13] T. C. Li, Y. V. Lim, X. S. Xie, X. L. Li, G. J. Li, D. L. Fang, Y. F. Li, Y. S. Ang, L. K. Ang, H. Y. Yang, *Small* **2021**, *17*, 2101728.
[14] Y. X. Zeng, X. Y. Zhang, R. F. Qin, X. Q. Liu, P. P. Fang, D. Z. Zheng, Y. X. Tong, X. H. Lu, *Adv. Mater.* **2019**, *31*, 201903675.

[15] Y. R. Zhou, X. N. Wang, X. F. Shen, Y. H. Shi, C. F. Zhu, S. Zeng, H. Xu, P. Cao, Y. L. Wang, J. T. Di, Q. W. Li, *J. Mater. Chem. A* **2020**, *8*, 11719.
[16] W. Li, Y. S. Ma, P. Li, X. Y. Jing, K. Jiang, D. H. Wang, *Adv. Energy Mater.* **2021**, *11*, 2102607.
[17] Y. Yang, J. F. Xiao, J. Y. Cai, G. M. Wang, W. C. Du, Y. F. Zhang, X. H. Lu, C. C. Li, *Adv. Funct. Mater.* **2021**, *31*, 2005092.
[18] S. L. Liu, J. F. Mao, W. K. Pang, J. Vongsvivut, X. H. Zeng, L. Thomsen, Y. Y. Wang, J. W. Liu, D. Li, Z. P. Guo, *Adv. Funct. Mater.* **2021**, *31*, 202104281.
[19] X. H. Zeng, J. F. Mao, J. N. Hao, J. T. Liu, S. L. Liu, Z. J. Wang, Y. Y. Wang, S. L. Zhang, T. Zheng, J. W. Liu, P. H. Rao, Z. P. Guo, *Adv. Mater.* **2021**, *33*, 202007416.
[20] X. H. Zeng, J. T. Liu, J. F. Mao, J. N. Hao, Z. J. Wang, S. Zhou, C. D. Ling, Z. P. Guo, *Adv. Energy Mater.* **2020**, *10*, 201904163.
[21] X. Y. Wu, Y. K. Xu, C. Zhang, D. P. Leonard, A. Markir, J. Lu, X. L. Ji, *J. Am. Chem. Soc.* **2019**, *141*, 6338.
[22] S. Y. Cai, X. Y. Chu, C. Liu, H. W. Lai, H. Chen, Y. Q. Jiang, F. Guo, Z. K. Xu, C. S. Wang, C. Gao, *Adv. Mater.* **2021**, *33*, 2007470.
[23] Q. Zhang, Y. L. Ma, Y. Lu, L. Li, F. Wan, K. Zhang, J. Chen, *Nat. Commun.* **2020**, *11*, 4463.
[24] L. Zhang, I. A. Rodriguez-Perez, H. Jiang, C. Zhang, D. P. Leonard, Q. B. Guo, W. F. Wang, S. M. Han, L. M. Wang, X. L. Ji, *Adv. Funct. Mater.* **2019**, *29*, 1902653.
[25] F. Wang, O. Borodin, T. Gao, X. Fan, W. Sun, F. Han, A. Faraone, J. A. Dura, K. Xu, C. Wang, *Nat. Mater.* **2018**, *17*, 543.
[26] Y. H. Shen, B. Liu, X. R. Liu, J. Liu, J. Ding, C. Zhong, W. B. Hu, *Energy Storage Mater.* **2021**, *34*, 461.
[27] S. Guo, L. P. Qin, T. S. Zhang, M. Zhou, J. Zhou, G. Z. Fang, S. Q. Liang, *Energy Storage Mater.* **2021**, *34*, 545.
[28] Y. Yamada, J. H. Wang, S. Ko, E. Watanabe, A. Yamada, *Nat. Energy* **2019**, *4*, 269.
[29] J. N. Hao, X. L. Li, X. H. Zeng, D. Li, J. F. Mao, Z. P. Guo, *Energy Environ. Sci.* **2020**, *13*, 3917.
[30] J. N. Hao, L. B. Yuan, C. Ye, D. L. Chao, K. Davey, Z. P. Guo, S. Z. Qiao, *Angew. Chem., Int. Ed.* **2021**, *60*, 7366.
[31] R. Z. Qin, Y. T. Wang, M. Z. Zhang, Y. Wang, S. X. Ding, A. Y. Song, H. C. Yi, L. Y. Yang, Y. L. Song, Y. H. Cui, J. Liu, Z. Q. Wang, S. N. Li, Q. H. Zhao, F. Pan, *Nano Energy* **2021**, *80*, 105478.
[32] N. N. Chang, T. Y. Li, R. Li, S. N. Wang, Y. B. Yin, H. M. Zhang, X. F. Li, *Energy Environ. Sci.* **2020**, *13*, 3527.
[33] L. S. Cao, D. Li, E. Y. Hu, J. J. Xu, T. Deng, L. Ma, Y. Wang, X. Q. Yang, C. S. Wang, *J. Am. Chem. Soc.* **2020**, *142*, 21404.
[34] Q. S. Nian, X. R. Zhang, Y. Z. Feng, S. Liu, T. J. Sun, S. B. Zheng, X. D. Ren, Z. L. Tao, D. H. Zhang, J. Chen, *ACS Energy Lett.* **2021**, *6*, 2174.
[35] M. D. Yan, N. Dong, X. S. Zhao, Y. Sun, H. L. Pan, *ACS Energy Lett.* **2021**, *6*, 3236.
[36] G. Z. Jia, F. Wang, X. Q. Yang, J. Qian, *J. Mol. Liq.* **2014**, *197*, 328.
[37] V. Balos, S. Imoto, R. R. Netz, M. Bonn, D. J. Bonthuis, Y. Nagata, J. Hunger, *Nat. Commun.* **2020**, *11*, 1611.
[38] J. Self, B. M. Wood, N. N. Rajput, K. A. Persson, *J. Phys. Chem. C* **2018**, *122*, 1990.
[39] M. Mohsen-Nia, H. Amiri, B. Jazi, *J. Solution Chem.* **2010**, *39*, 701.
[40] Q. Zhang, K. X. Xia, Y. L. Ma, Y. Lu, L. Li, J. Liang, S. L. Chou, J. Chen, *ACS Energy Lett.* **2021**, *6*, 2704.
[41] M. Smiechowski, J. Stangret, *J. Mol. Struct.* **2008**, *878*, 104.
[42] P. Sun, L. Ma, W. H. Zhou, M. J. Qiu, Z. L. Wang, D. L. Chao, W. J. Mai, *Angew. Chem., Int. Ed.* **2021**, *60*, 18247.
[43] Z. Zhao, J. Zhao, Z. Hu, J. Li, J. Li, Y. Zhang, C. Wang, G. Cui, *Energy Environ. Sci.* **2019**, *12*, 1938.
[44] A. Pei, G. Y. Zheng, F. F. Shi, Y. Z. Li, Y. Cui, *Nano Lett.* **2017**, *17*, 1132.
[45] L. Oniciu, L. Muresan, *J. Appl. Electrochem.* **1991**, *21*, 565.
[46] W. H. Yang, X. F. Du, J. W. Zhao, Z. Chen, J. J. Li, J. Xie, Y. J. Zhang, Z. L. Cui, Q. Y. Kong, Z. M. Zhao, C. G. Wang, Q. C. Zhang, G. L. Cui, *Joule* **2020**, *4*, 1557.
[47] T. T. Wang, C. P. Li, X. S. Xie, B. G. Lu, Z. X. He, S. Q. Liang, J. Zhou, *ACS Nano* **2020**, *14*, 16321.
[48] T. P. Jiao, Q. Yang, S. L. Wu, Z. F. Wang, D. Chen, D. Shen, B. Liu, J. Y. Cheng, H. F. Li, L. T. Ma, C. Y. Zhi, W. J. Zhang, *J. Mater. Chem. A* **2019**, *7*, 16330.
[49] P. He, M. Y. Yan, G. B. Zhang, R. M. Sun, L. N. Chen, Q. Y. An, L. Q. Mai, *Adv. Energy Mater.* **2017**, *7*, 1601920.
[50] J. P. Liu, W. C. Peng, Y. Li, F. B. Zhang, X. B. Fan, *J. Mater. Chem. C* **2021**, *9*, 6308.
[51] W. W. Xu, C. L. Sun, K. N. Zhao, X. Cheng, S. Rawal, Y. Xu, Y. Wang, *Energy Storage Mater.* **2019**, *16*, 527.